Assessment of phantom dosimetry and image quality of i-CAT FLX cone-beam computed tomography

John B. Ludlow[a] and Cameron Walker[b]
Chapel Hill, NC, and Kansas City, Mo

Introduction: The increasing use of cone-beam computed tomography in orthodontics has been coupled with heightened concern about the long-term risks of x-ray exposure in orthodontic populations. An industry response to this has been to offer low-exposure alternative scanning options in newer cone-beam computed tomography models. **Methods:** Effective doses resulting from various combinations of field of view size and field location comparing child and adult anthropomorphic phantoms with the recently introduced i-CAT FLX cone-beam computed tomography unit (Imaging Sciences, Hatfield, Pa) were measured with optical stimulated dosimetry using previously validated protocols. Scan protocols included high resolution (360° rotation, 600 image frames, 120 kV[p], 5 mA, 7.4 seconds), standard (360°, 300 frames, 120 kV[p], 5 mA, 3.7 seconds), QuickScan (180°, 160 frames, 120 kV[p], 5 mA, 2 seconds), and QuickScan+ (180°, 160 frames, 90 kV[p], 3 mA, 2 seconds). Contrast-to-noise ratio was calculated as a quantitative measure of image quality for the various exposure options using the QUART DVT phantom. **Results:** Child phantom doses were on average 36% greater than adult phantom doses. QuickScan+ protocols resulted in significantly lower doses than standard protocols for the child ($P = 0.0167$) and adult ($P = 0.0055$) phantoms. The 13 × 16-cm cephalometric fields of view ranged from 11 to 85 μSv in the adult phantom and 18 to 120 μSv in the child phantom for the QuickScan+ and standard protocols, respectively. The contrast-to-noise ratio was reduced by approximately two thirds when comparing QuickScan+ with standard exposure parameters. **Conclusions:** QuickScan+ effective doses are comparable with conventional panoramic examinations. Significant dose reductions are accompanied by significant reductions in image quality. However, this trade-off might be acceptable for certain diagnostic tasks such as interim assessment of treatment results. (Am J Orthod Dentofacial Orthop 2013;144:802-17)

The use of cone-beam computed tomography (CBCT) in orthodontics has increased dramatically over the last few years.[1] Because cancer is the principal long-term biologic effect of exposure to x-rays, one of the greatest issues facing use of CBCT in orthodontics is justification of the increased doses of ionizing radiation administered to patients compared with standard 2-dimensional imaging techniques.

A routine medical computed tomography head scan can have an effective dose of approximately 2 mSv.[2] Whereas most CBCT examinations have been reported to impart a much lower dose, CBCT units from different manufacturers vary in their doses by as much as 10-fold for an equivalent field of view (FOV), with some units roughly equivalent in dose to optimized computed tomography scans.[3] Although the risk to a patient from 1 computed tomography or CBCT examination might not by itself be large, millions of examinations are performed each year, making radiation exposure from dental and medical imaging an important public health issue. It has been estimated that 1.5% to 2% of all cancers in the United States can be attributed to computed tomography studies alone.[4] This is especially important for the adolescent and pediatric populations that routinely receive orthodontic treatment and whose

[a]Professor, Department of Diagnostic Sciences, School of Dentistry, University of North Carolina, Chapel Hill, NC.
[b]Adjunct assistant professor, Faculty of Orthodontics, School of Dentistry, University of Missouri, Kansas City, Mo.
The authors have completed and submitted the ICMJE Form for Disclosure of Potential Conflicts of Interest, and none were reported.
Travel support and an honorarium were provided to Dr Ludlow by Imaging Sciences, Hatfield, Pa.
Supported in part by the National Institute of Dental and Craniofacial Research of the National Institutes of Health under award number R21DE022160. The content is solely the responsibility of the authors and does not necessarily represent the official views of the National Institutes of Health.
Address correspondence to: John B. Ludlow, North Carolina Oral Health Institute, Koury Oral Health Sciences, Room 5411-K, 385 S Columbia St, Chapel Hill, NC 27599-7455; e-mail, jbl@email.unc.edu.
Submitted, May 2013; revised and accepted, July 2013.
0889-5406/$36.00

http://dx.doi.org/10.1016/j.ajodo.2013.07.013

Table I. Dosimetry plan for recording of adult and child phantom effective dose for i-CAT Next Generation programs and exposure settings

FOV (cm)	ROI	Protocol	Scan angle (°)	Basis image frames (n)	Voxel size (mm)	Adult phantom	Child phantom	kV(p)	mA	Exposure (s)
8 × 8	Dental	QuickScan+	180	160	0.3*/0.4	A	C	90	3	2.0
16 × 6	Maxilla	QuickScan+	180	160	0.3*/0.4	A	C	90	3	2.0
16 × 6	Mandible	QuickScan+	180	160	0.3*/0.4	A	C	90	3	2.0
16 × 8	Both arches	QuickScan+	180	160	0.3*/0.4	A	C	90	3	2.0
16 × 11	Arches + TMJ	QuickScan+	180	160	0.3*/0.4	A	C	90	3	2.0
16 × 13	Standard ceph	QuickScan+	180	160	0.3*/0.4	A	C	90	3	2.0
16 × 6	Maxilla	QuickScan	180	160	0.3*/0.4	A	C	120	5	2.0
8 × 8	Dental	QuickScan	180	160	0.3*/0.4	A	C	120	5	2.0
16 × 13	Standard ceph	QuickScan	180	160	0.3*/0.4	A	C	120	5	2.0
16 × 8	Both arches	QuickScan	180	160	0.3*/0.4	A	C	120	5	2.0
16 × 11	Arches + TMJ	QuickScan	180	160	0.3*/0.4	A	C	120	5	2.0
16 × 6	Mandible	QuickScan	180	160	0.3*/0.4	A	C	120	5	2.0
8 × 8	Dental	Standard	360	300	0.3*/0.4	A	C	120	5	3.7
16 × 6	Maxilla	Standard	360	300	0.3*/0.4	A	C	120	5	3.7
16 × 6	Mandible	Standard	360	300	0.3*/0.4	A	C	120	5	3.7
16 × 8	Both arches	Standard	360	300	0.3*/0.4	A	C	120	5	3.7
16 × 11	Arches + TMJ	Standard	360	300	0.3*/0.4	A	C	120	5	3.7
16 × 13	Standard ceph	Standard	360	300	0.3*/0.4	A	C	120	5	3.7
8 × 8	Dental	High resolution	360	600	0.125*/0.20/0.25	A		120	5	7.4
16 × 6	Maxilla	High resolution	360	600	0.125/0.20*/0.25	A		120	5	7.4
16 × 6	Mandible	High resolution	360	600	0.125/0.20*/0.25	A		120	5	7.4
16 × 8	Both arches	High resolution	360	600	0.125/0.20*/0.25	A		120	5	7.4
16 × 11	Arches + TMJ	High resolution	360	600	0.125/0.20/0.25*	A		120	5	7.4
16 × 13	Standard ceph	High resolution	360	600	0.125/0.20*/0.25	A		120	5	7.4
23 × 17	EFOV	Standard	360	300	0.3*/0.4	A		120	5	3.7
23 × 17	EFOV	Enhanced	360	600	0.3*/0.4	A		120	5	7.4

ROI, Region of interest; *TMJ*, temporomandibular joint; *ceph*, cephalometric; *EFOV*, extended field of view.
*Actual voxel size used in this study.

cellular growth and organ development are associated with increased radiosensitivity of tissues. In conjunction with a longer life expectancy in which cancer can develop, children are 2 to 5 times more sensitive to radiation carcinogenesis than mature adults.[2,5]

Image quality in CBCT is observer dependent, subjective, and used to describe how well the desired information can be extracted from an image. Because it is subjective, the measurement and comparison of image quality across CBCT units in diagnostic situations are complex problems. Two elements of subjective image quality that correlate with objective quality measures include contrast and spatial resolution.[6] Image contrast can be objectively measured with the contrast-to-noise ratio, and spatial resolution can be measured by computing a modulation transfer function. The quality of CBCT scans is also an important consideration for users in orthodontics because the selection of image quality for a CBCT scan becomes a decision on dose and vice versa. Image quality technical-factor adjustments that select between "high" and "low" image quality in many CBCT units can cause as much as a 7-fold difference in doses.[3]

The ongoing challenge in the optimization of CBCT is to reduce the dose without drastically decreasing image quality and diagnostic information. One potential means of reducing patient risk from CBCT examinations is to limit the area of exposure using variable FOVs that are sized for the location of the anatomy of interest. However, voxel size is linked to FOV in many CBCT units, and smaller voxel sizes associated with smaller FOVs can actually increase the dose because of increases in exposure that are needed to maintain an adequate contrast-to-noise ratio. Another approach is to reduce exposure for diagnostic tasks that theoretically require lower contrast-to-noise ratios or lower signal modulation transfer functions. An example of this type of task might be checking the angulation of roots. The combination of careful selection of exposure parameters and FOV can result in an optimal dose for specific diagnostic tasks in orthodontic practice.

The purpose of this study was to evaluate doses resulting from various combinations of FOV size, location, and exposure parameters using child and adult phantoms with the i-CAT FLX unit (Imaging Sciences, Hatfield, Pa). A second aim was to measure contrast-to-noise ratio and modulation transfer function as quantitative

OSL ID No.	Adult Phantom Location (level of OSLD location)
1	Calvarium anterior (2)
2	Mid brain (2)
3	Calvarium left (3)
4	Mid brain (3)
5	Calvarium posterior (4)
6	Pituitary (4)
7	Right lens of eye (4-5)
8	Left lens of eye (4-5)
9	Right ethmoid (5
10	Left maxillary sinus (6)
11	Oropharyngeal airway (7)
12	Right parotid (7)
13	Left parotid (7)
14	Right ramus (7)
15	Left ramus (7)
16	Left back of neck (8)
17	Right submandibular gland (8)
18	Left submandibular gland (8)
19	Center sublingual gland (8)
20	Center C spine (8)
21	Lateral neck - left (9)
22	Thyroid – left (10)
23	Thyroid - right (10)
24	Esophagus (10)

Fig 1. Locations of optically stimulated luminescent dosimeters (*OSLD*) in adult ATOM Max model 711 phantom.

measurements of image quality for the various exposure options offered by the i-CAT unit. A tertiary aim was to compare phantom sizes and types as well as thermoluminescent dosimetry and optically stimulated luminescent (OSL) dosimetry.

MATERIAL AND METHODS

OSL dosimeters (Nanodot; Landauer, Glenwood, Ill) are plastic disks infused with aluminum oxide doped with carbon (Al_2O_3:C). The trace amounts of carbon in the aluminum oxide crystal lattice create imperfections that act as traps (F centers) for electrons and positively charged areas called "holes." After exposure to ionizing radiation, free electrons and holes are generated and trapped at the F centers in proportion to the amount of energy in the exposure. Energy captured by the F centers is reemitted as light when electrons and holes recombine. Recombination occurs when the crystal is optically stimulated with a controlled exposure of 540-nm light from a light-emitting diode. The energy released from the F centers can be distinguished from the stimulating light because it is emitted in the form of 420-nm photons. The intensity or quantity of the emitted photons depends on the dose absorbed by the OSL dosimeter and the controlled intensity of the stimulating light. The intensity of the emitted light is proportional to the stored dose and is recorded by a photomultiplier tube that incorporates a filter that screens out photons from the stimulating light source. Each dosimeter is encased in a light-tight plastic holder measuring approximately 1 × 10 × 10 mm. This case prevents loss of energy through stimulation by ambient light. Dosimeters used in this study were read with a portable reader (MicroStar; Landauer). The reader was calibrated before use. After calibration, photon counts from dosimeters can be recorded with an accuracy of about ±2%. Photon counts are converted to doses using an energy-specific conversion factor. Doses reported by the reader were adjusted for energy response using a third-order polynomial calibration curve derived from side-by-side comparisons of recorded doses from an ion chamber and OSL dosimeters over a range of 80 to 120 kV(p) using an adjustable kilovolt peak source. For this study, the OSL sensitivity at 90 kV(p) was estimated at .94 (mean, 60 kV). OSL sensitivity at 120 kV(p) was estimated at 0.78 (mean, 80 kV).

A software and hardware upgraded model of the i-CAT Next Generation dental CBCT unit (Imaging Sciences) was investigated in this study. It was updated to meet specifications that were named "i-CAT FLX." Volume scans for this unit ranged from 8 × 8 cm to 23 × 17 cm. The unit operates at 90 or 120 kV(p) and 3 or 5 mA with a pulsed exposure time from 2.0 to 7.4

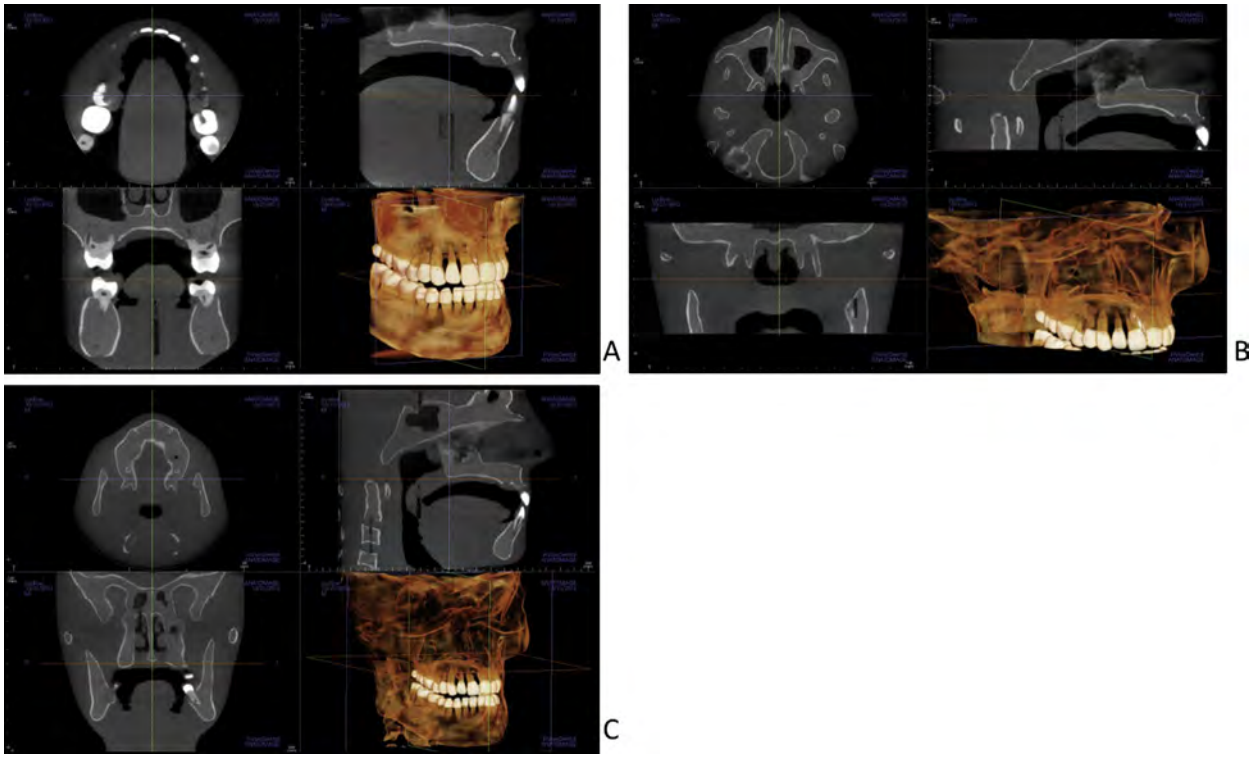

Fig 2. Adult phantom demonstrating positioning principles for phantom scanning. **A,** The lower border of volume is 5 mm below the bony chin; the anterior border of volume is 5 mm anterior to the central incisors. This positioning was used on dental (8 × 8-cm high-resolution scan here), mandible, both arches, and arches + temporomandibular joint scans. **B,** The lower border of volume is 5 mm below the central incisal edge; the anterior border of volume is 5 mm anterior to the central incisors. This positioning was used on maxilla volumes (6 × 16-cm high-resolution scan here). **C,** The tip of the nose and the lower soft-tissue border of the chin are included in the FOV for standard cephalometric volumes (13 × 16-cm high-resolution scan here) and extended FOV volumes.

seconds. The unit rotates through 360° over 8.6 or 26 seconds. A 180° rotation is also available with a rotation time of 4.8 seconds. The scan parameters used for scans of the child and adult phantoms are given in Table I.

Adult dosimetry was acquired using a tissue-equivalent phantom simulating the anatomy of an average adult male (ATOM Max model 711 HN; CIRS, Norfolk, Va). The phantom includes detailed 3-dimensional anthropomorphic anatomy including brain, bone, larynx, trachea, sinus, nasal cavities, and teeth. The bones contain both cortical and trabecular separations. The phantom was modified by machining slots to accept nanodot dosimeters at sites corresponding to the internal tissues of interest. A skin surface dosimeter in the back of the neck was positioned at the vertical center of the designated slice level and taped in position. Lens of eye dosimeters were centered over and inset in the anatomic location for the lens and taped in position. Internal dosimeters were positioned vertically with the upper edge of the dosimeter slot, flush with the surface of the selected slice level, and held in position by friction of the dosimeter case and the phantom material at the sampled anatomic location. Adult dosimeter anatomic locations and phantom levels are shown in Figure 1. During scanning, the phantom was oriented with its section planes approximately parallel to the scan rotation plane (horizon). A phantom position simulating the positioning of a patient on the chin rest was used. With the exception of the 13 × 16-cm cephalometric and 6 × 16-cm maxillary FOVs, centered FOVs were positioned to capture approximately 5 mm of soft tissue below the lower cortical border of the chin. The anteroposterior position of the phantom was established to capture approximately 5 mm of soft tissue anterior to the facial surface of the maxillary incisor crowns. For the 6 × 16-cm maxillary views, the lower border of the FOV was positioned approximately 5 mm below the maxillary central incisor edge. For the 13 × 16-cm cephalometric views, the tip of the nose and the lower soft tissue border of the chin were included in the FOV (Fig 2).

OSL ID No.	Child Phantom Location (level of OSLD location)
1	Calvarium anterior (2)
2	Calvarium left (2)
3	Calvarium posterior (2)
4	Mid brain (2)
5	Mid brain (3)
6	Pituitary (4)
7	Right orbit (4)
8	Right lens of eye (4-5)
9	Left lens of eye (4-5)
10	Right maxillary sinus (5)
11	Left nasal airway (5)
12	Right parotid (6)
13	Left parotid (6)
14	Left back of neck (6)
15	Right ramus (7)
16	Left ramus (7)
17	Right submandibular gland (7)
18	Left submandibular gland (7)
19	Center sublingual gland (7)
20	Center C spine (8)
21	Thyroid superior–left (8)
22	Thyroid – left (9)
23	Thyroid - right (9)
24	Esophagus (9)

Fig 3. Ten-year-old child phantom dosimeter locations.

Child dosimetry was acquired using a tissue-equivalent phantom simulating the anatomy of a 10-year-old child (ATOM model 706 HN; CIRS). Tissues simulated in this phantom were average soft tissue, average bone tissue, spinal cord, spinal discs, brain, and sinus. Simulated bone tissue matches age-related density. Dosimeter anatomic locations and child phantom levels are shown in Figure 3. With the exception of the 11 × 16-cm, 13 × 16-cm, and 6 × 16-cm maxillary FOVs, centered FOVs were positioned to capture approximately 5 mm of soft tissue below the lower cortical border of the chin. The anteroposterior position of the phantom was established to capture approximately 5 mm of soft tissue anterior to the facial surface of the maxillary incisor crown. For the 6 × 16-cm maxillary views, the lower border of the FOV was positioned approximately 5 mm below the maxillary central incisor edge. For the 11 × 16-cm and 13 × 16-cm cephalometric views, the tip of the nose and the lower soft tissue border of the chin were included in the FOV (Fig 4).

Two to 12 exposures were used for each dosimeter run to provide a more reliable measure of radiation in the dosimeters. Smaller FOVs required more exposure repetitions because more dosimeters are outside the field of direct exposure and absorb only small quantities of scatter radiation. For every scan, a scout view was also acquired. Doses recorded by the OSL dosimetry reader were divided by the number of scans to determine the exposure per examination for each dosimeter.

Doses recorded by OSL dosimeters at different positions in a tissue or an organ were averaged to express the average tissue-absorbed dose in micrograys. The products of these values and the percentage of a tissue or an organ irradiated in a radiographic examination (Table II) were used to calculate the equivalent dose in microsieverts.[7]

For bone, the equivalent dose to the whole-body bone surface was calculated using the summation of the individual equivalent doses to the calvarium, mandible, and cervical spine. The determination of these equivalent doses was based on the distribution of bone throughout the body: the mandible contains 1.3%, the calvaria, 11.8%, and the cervical spine, 3.4%.[8] Distribution of adult bone marrow was calculated using an average of data from Christy[9] for 25- and 40-year-olds. The mandible contains 0.8%, the calvaria, 7.7%, and the cervical spine, 3.8% of the adult marrow distribution. The 10-year-old child's marrow distribution was calculated as 1.1% for the mandible, 11.6% for the cranium, and 2.7% for the cervical spine, for a total of 15.4% of the total body marrow. With the

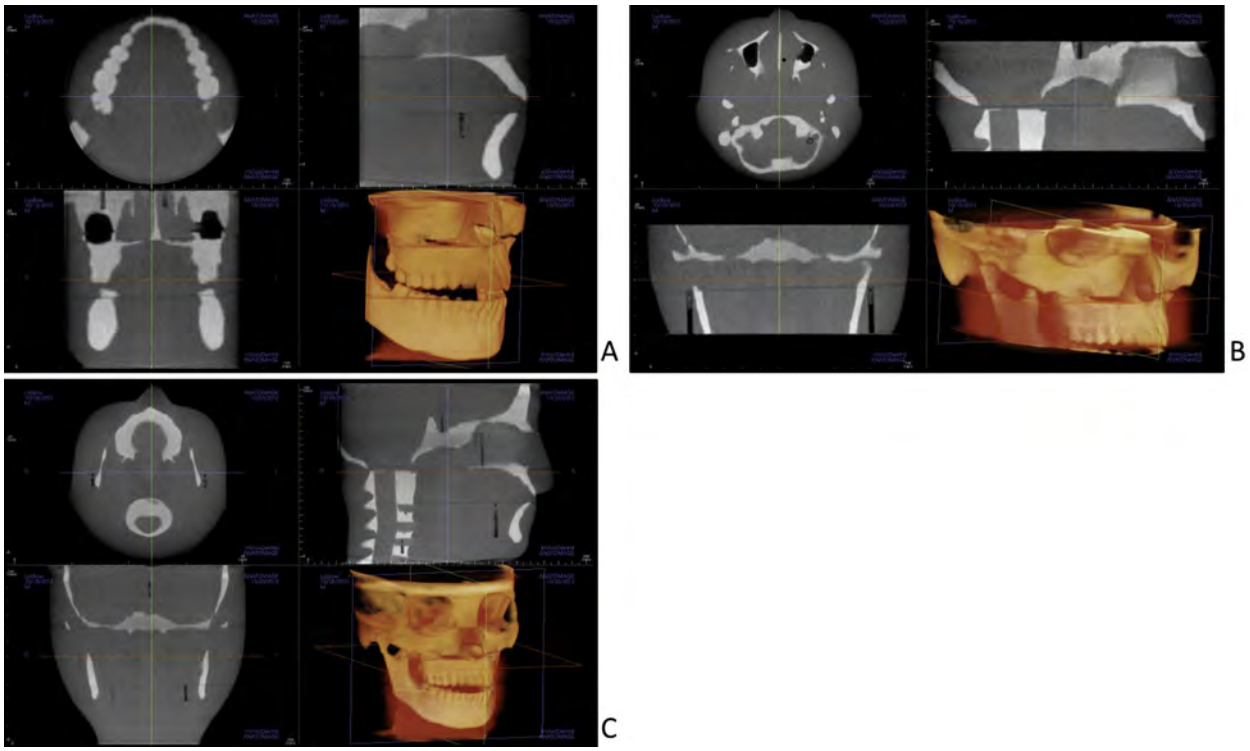

Fig 4. Child phantom demonstrating positioning principles for phantom scanning. **A,** The lower border of volume is 5 mm below the bony chin; the anterior border of volume is 5 mm anterior to the central incisors. This positioning was used on dental (8 × 8-cm high-resolution scan here), mandible, and both arches. **B,** The lower border of volume is 5 mm below the central incisal edge; the anterior border of volume is 5 mm anterior to the central incisors. This positioning was used on maxilla volumes (6 × 16-cm high-resolution scan here). **C,** The tip of the nose and lower soft-tissue border of the chin are included in the FOV for standard cephalometric volumes (13 × 16-cm high-resolution scan here) and arches + temporomandibular joint scans.

technique of Underhill et al,[8] 3 locations in the calvarium were averaged to determine the calvarial dose. For bone, a correction factor based on experimentally determined mass energy attenuation coefficients for bone and muscle irradiated with mono-energetic photons was applied. An effective beam energy estimated to be two thirds of the peak beam energy of the x-ray unit was used to determine the bone-to-muscle attenuation ratios. A linear fit (R^2 = 0.996) of ratios from 40 to 80 kV from published data produced the following equation: bone-to-muscle attenuation ratio = −0.0618 × kV(p) × 2/3 + 6.9406.[10] Values calculated from this equation provided bone-to-muscle attenuation ratios of 3.21 at 60 kV (90 kV[p]) and 1.97 at 80 kV (120 kV[p]).

The proportion of skin surface area in the head and neck region directly exposed during maxillofacial CBCT imaging is estimated at 5% of the total body to calculate the radiation-weighted dose to the skin following the procedure Ludlow et al.[11] Similarly, muscle and lymphatic nodes exposures are estimated to represent 5% of the total body complement for these tissues. The proportion of the esophageal tract that is exposed was set at 10%. Other tissues of interest were calculated at 100%.

The effective dose is a calculation that permits comparison of the detriment of different exposures to ionizing radiation to an equivalent detriment produced by a full-body dose of radiation. Effective dose, expressed in microsieverts, is calculated with the equation: $E = \sum w_T \times H_T$, where E is the summation of the products of the tissue weighting factor (w_T), which represents the relative contribution of that organ or tissue to the overall risk, and the radiation weighted dose H_T.[7] The whole-body risk is determined by the summation of the radiation-weighted doses to all tissues or organs exposed. International Commission on Radiological Protection weighting factors in Table II were used to calculate the effective doses.[7]

Tissue weighting factors used in the International Commission on Radiological Protection calculation of

Table II. Estimated percentage of tissue irradiated, International Commission on Radiological Protection weighting factor for calculation of effective dose, and TLDs used to calculate the mean absorbed doses to a tissue or an organ of an adult or a 10-year-old child phantom

	Fraction irradiated adult (%)	*OSL ID (Fig 1)*	*ICRP 2007 w_T*	*Fraction irradiated child (%)*	*OSL ID (Fig 3)*
Bone marrow	12.2		0.12	15.4	
Mandible	0.8	14, 15		1.1	15, 16
Calvaria	7.7	1, 3, 5		11.6	1, 2, 3
Cervical spine	3.8	20		2.7	20
Thyroid	100	22, 23	0.04	100	21, 22, 23
Esophagus	10	24	0.04	10	24
Skin	5	7, 8, 16	0.01	5	8, 9, 14
Bone surface*	16.5		0.01	16.5	
Mandible	1.3	14, 15		1.3	15, 16
Calvaria	11.8	1, 3, 5		11.8	1, 2, 3
Cervical spine	3.4	20		3.4	20
Salivary glands	100		0.01	100	
Parotid	100	12, 13		100	12, 13
Submandibular	100	17, 18		100	17, 18
Sublingual	100	19		100	19
Brain	100	2, 4, 6	0.01	100	4, 5, 6
Remainder			0.12		
Lymphatic nodes	5	11-13, 17-19, 21-24		5	12-13, 17-19, 21-24
Muscle	5	11-13, 17-19, 21-24		5	12-13, 17-19, 21-24
Extrathoracic region	100	9-13, 17-19, 21-24		100	10-13, 17-19, 21, 24
Oral mucosa	100	11-13, 17-19		100	12-13, 17-19

OSL ID, OSL dosimeter identification number; *ICRP*, International Commission on Radiological Protection.
*Bone surface dose = bone marrow dose × bone/muscle mass energy absorption coefficient ratio = −0.0618 × 2/3 kV(p) + 6.9406 using data taken from NBS Handbook 85.[10]

effective dose include 14 independently weighted tissues and 14 remainder tissues.[8] Because the uterus and the cervix are present only in females, and the prostate only in males, the number used in the weighted averaging of the remainder tissues was 13.

In previous studies, a radiation analog dosimetry system (RANDO) phantom (Nuclear Associates, Hicksville, NY) and thermoluminescent dosimeters (TLDs) have commonly been used for dosimetry.[3,11] Because each RANDO phantom is formed around an actual human skull, the attenuation characteristics for each RANDO are variable. The precision-manufactured ATOM phantom was selected as a more reproducible model for comparative dosimetry. Effective doses were evaluated for standard and extended-field cephalometric data runs and for previously reported RANDO TLD data runs as well as for unreported OSL runs. These were compared with the adult ATOM phantom results of this study.

Analysis of variance (ANOVA) of effective dose results was used to assess data for significant differences caused by phantom type (adult or child), region of interest (dental, mandible, both arches, arches + temporomandibular joint, standard cephalometrics), and scan protocol (QuickScan+, QuickScan, standard, or high resolution). When significant differences were found, the Tukey HSD test was used to determine which factors were significantly different from other factors. An alpha value of 0.05 was chosen for all tests.

Image quality indicators associated with FOV, scanning angle, kilovolt (peak), and voxel size were acquired using a QUART DVT_AP phantom and QUART DVT_TEC software (QUART, Zorneding, Germany) (Fig 5). The phantom consisted of 16-cm-diameter cylindrical slabs of acrylic plastic with polyvinyl chloride and air elements configured to permit measurements of polymethylmethacrylate voxel, polymethylmethacrylate noise, homogeneity, contrast, contrast-to-noise ratio, modulation transfer function 10%, modulation transfer function 50%, and Nyquist frequency. The measurements were calculated in a user-guided, semiautomatic manner from 2 DICOM slices selected from the volume. Each volume was measured 3 times, and averages and standard deviations of each parameter were calculated.

RESULTS

Volumes produced by ATOM and RANDO adult phantoms for the 13 × 16-cm standard cephalometric and 17 × 23-cm extended FOVs are shown in Figure 6. An unbiased estimator of difference between pairs ([A-B]/[A+B]/2) demonstrated that OSL dosimeter

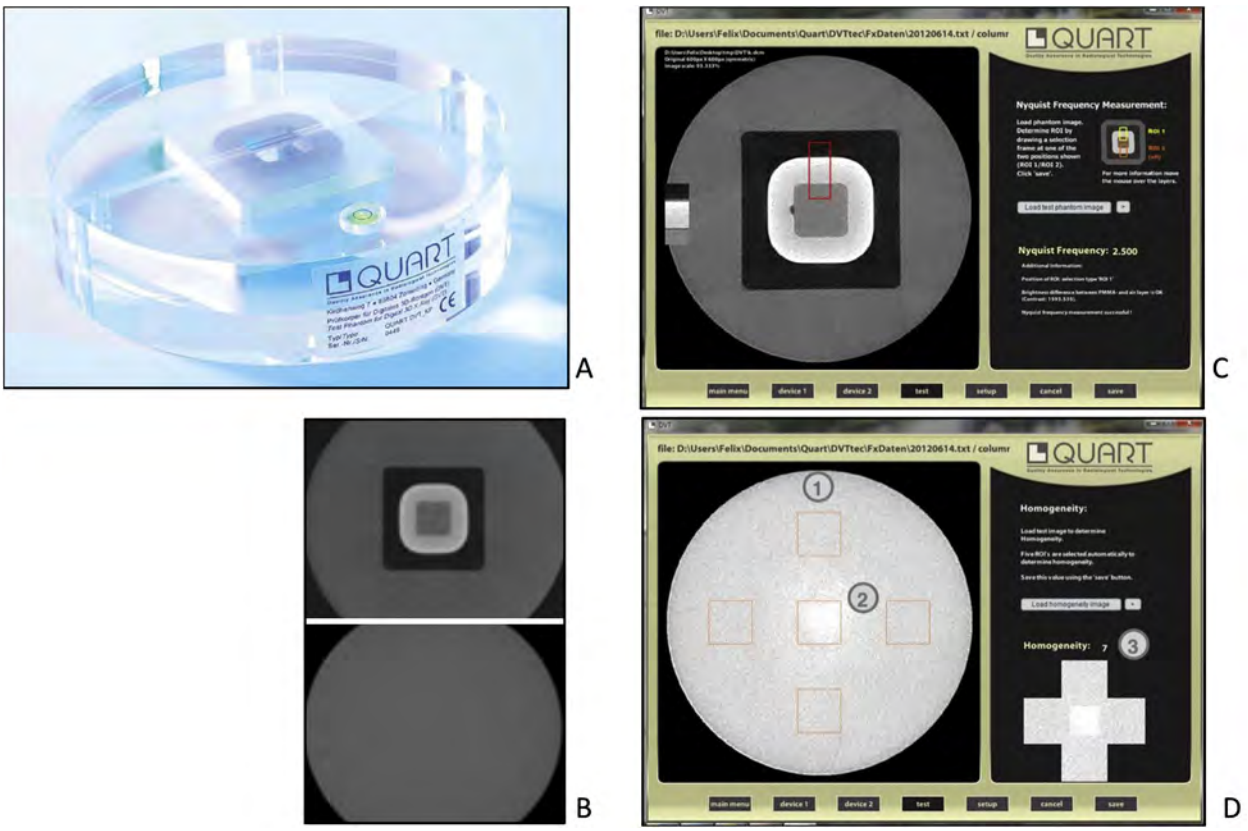

Fig 5. QUART DVT_AP CBCT image quality system: **A,** phantom; **B,** sample axial images of polyvinyl chloride and air elements (*top*) and acrylic plastic layer (*bottom*); **C,** analysis software window for calculation of the Nyquist frequency; **D,** analysis software window for calculating homogeneity.

readings were 1.0% less than thermoluminescent dosimetry readings for standard cephalometric fields and 2.5% less for extended FOV RANDO imaging. The adult ATOM phantom effective doses were 0.2% less than the RANDO doses for the standard cephalometric field and 0.8% less for the extended FOV.

ANOVA of the combined adult and child phantom effective dose data demonstrated significant differences caused by phantom ($P = 0.0026$), region of interest ($P < 0.0001$), and exposure protocol ($P < 0.0001$). Considering QuickScan+, QuickScan, and standard protocols, child phantom doses were on average 36% greater than adult phantom doses. Table III highlights the effective dose results for the adult phantom. The Tukey HSD test demonstrated that the QuickScan+ protocols resulted in significantly lower doses than the standard or high-resolution protocols but were not statistically different from the QuickScan protocols. The QuickScan protocol also resulted in lower doses than the high-resolution protocols but was not statistically different from the standard protocols. The 13 × 16-cm cephalometric imaging resulted in statistically higher doses than all other FOVs. Similarly, the 6 × 16-cm maxillary imaging resulted in significantly lower doses than all other fields. Results for the 17 × 23-cm extended FOV are not included in Table III because only standard and enhanced modes are available for this field. The effective doses were 69 μSv for the standard extended FOV and 136 μSv for the enhanced extended FOV.

Table IV highlights the effective dose results for the child phantom. The Tukey HSD test demonstrated that the each scan protocol was significantly different from the other protocols with increasing doses in order of QuickScan+, QuickScan, and standard protocols. Maxillary FOVs produced statistically lower doses than the arch + temporomandibular joint and the 13 × 16-cm cephalometric views.

Figure 7 is a graphic representation of the data in Table III. Figure 8 is a graphic representation of the data in Table IV.

Tables V and VI provide equivalent doses to tissues and organs used in the calculation of effective dose. Absorbed doses in the thyroid and brain were

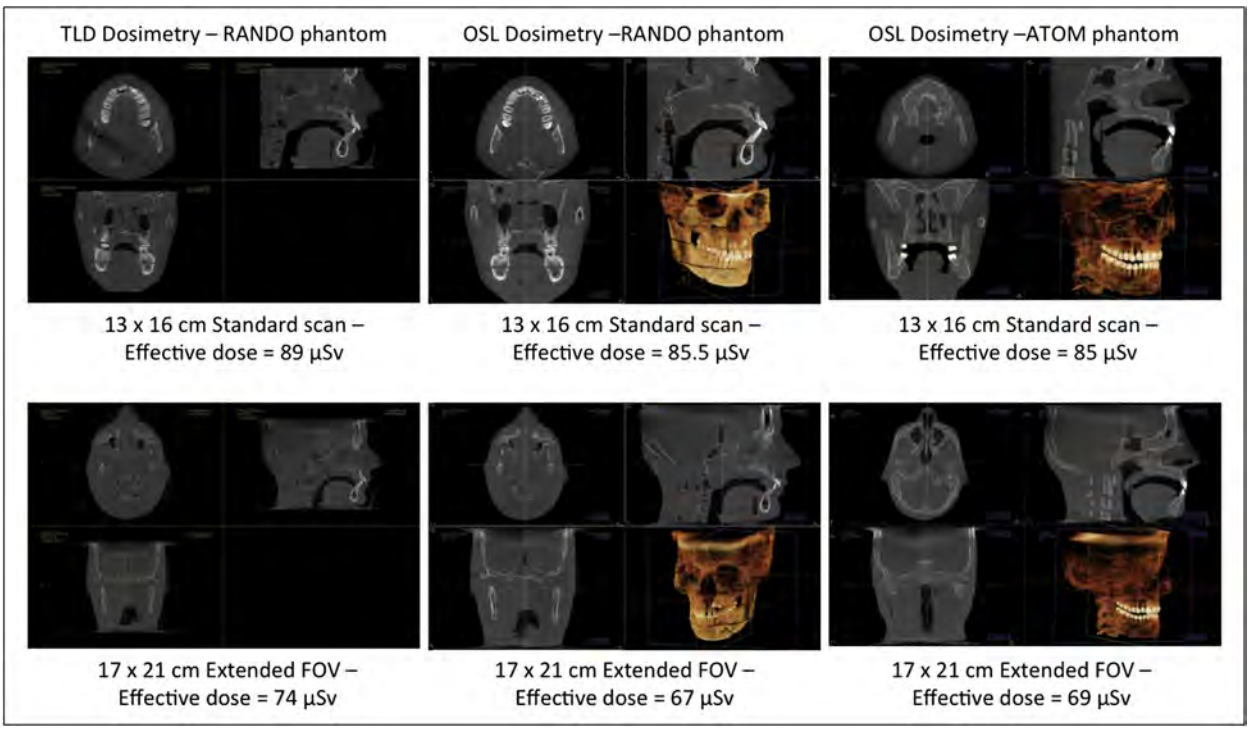

Fig 6. Comparison of RANDO and ATOM phantoms, TLDs and OSL dosimeters, and standard cephalometric and extended FOVs.

Table III. Effective doses (µSv) for the adult phantom by exposure protocol and FOV (ANOVA *P* value and Tukey HSD)

	Maxilla	*Dentition*	*Mandible*	*Both arches*	*Arches + TMJ*	*Standard ceph*	*Average*	*ANOVA P = 0.0055, Tukey HSD**
QuickScan+	4	5	8	8	9	11	8	C
QuickScan	20	23	34	39	43	54	36	BC
Standard	32	44	61	70	79	85	62	B
High resolution	65	85	127	148	159	171	126	A
Average	30	39	58	66	73	81	58	
ANOVA *P* <0.0001, Tukey HSD*	C	BC	ABC	ABC	AB	A		

TMJ, Temporomandibular joint; *ceph*, cephalometric.
*Levels not connected by same letter are significantly different.

significantly greater in the child phantom than in the adult phantom ($P < 0.0001$).

Table VII contains average parameter values and standard deviations from the analysis of the QUART phantom images.

Analysis with the QUART phantom demonstrated that increasing FOV diameter or increasing voxel size from 0.3 to 0.4 mm resulted in a 10% to 20% reduction in modulation transfer function. Modulation transfer function at 50% demonstrated a similar pattern of little response to milliamperes but provided a 17% reduction in modulation transfer function with either increased FOV diameter from 8 to 16 cm or increased voxel size from 0.3 to 0.4 mm. As expected, smaller voxel sizes resulted in higher modulation transfer function values or better resolution.

DISCUSSION

Most prior studies on CBCT dosimetry have used adult RANDO anthropomorphic phantoms.[3,12-14] However, variations in mass, organ volume, and organ position across the broad range of ages in the orthodontic patient population make it impossible to accurately estimate risk with 1 type of dosimetry

Table IV. Effective doses (μSv) for the child phantom by exposure protocol and FOV (ANOVA *P* value and Tukey HSD)

	Maxilla	*Dental*	*Mandible*	*Both arches*	*Arches + TMJ*	*Standard ceph*	*Average*	*ANOVA P = 0.0167, Tukey HSD**
QuickScan+	5	7	9	12	13	18	11	A
QuickScan	23	34	43	50	56	70	46	B
Standard	39	60	73	85	115	120	82	C
Average	22	34	42	49	61	69	46	
ANOVA *P* <0.0001, Tukey HSD*	B	AB	AB	AB	A	A		

TMJ, Temporomandibular joint; *ceph*, cephalometric.
*Levels not connected by same letter are significantly different.

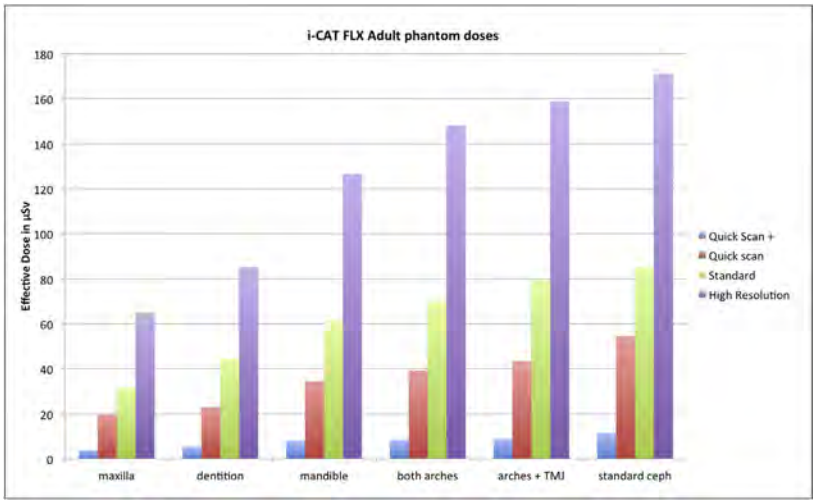

Fig 7. Adult phantom effective dose by scan type and FOV.

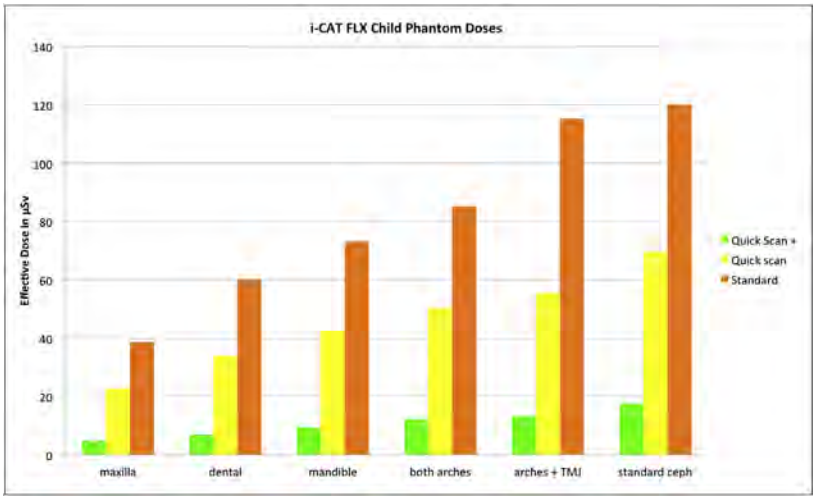

Fig 8. Depiction of child phantom effective dose by exposure protocol and FOV.

Table V. Equivalent dose measurements (μGy) on an adult phantom for i-CAT FLX by FOV, region of interest, and scanning protocol

				Weighted components of effective dose calculation group components								*Remainder group components*			
FOV (cm)	*Region of interest*	*Protocol*	*Effective dose (μSv)*	*Bone marrow*	*Thyroid*	*Esophagus*	*Skin*	*Bone surface*	*Salivary glands*	*Brain*	*Remainder average*	*Lymphatic nodes*	*Extrathoracic airway*	*Muscle*	*Oral mucosa*
8 × 8	Dentition	QuickScan+	5.3	4	22	2	2	15	142	4	18	5	90	5	133
16 × 6	Maxilla	QuickScan+	3.9	4	9	1	1	15	96	13	15	4	73	3	112
16 × 6	Mandible	QuickScan+	8.1	9	36	5	4	30	193	6	25	7	121	7	195
16 × 8	Both arches	QuickScan+	8.5	9	38	5	4	32	196	9	27	7	132	7	200
16 × 11	Arches + TMJ	QuickScan+	8.8	9	36	4	5	33	207	19	29	8	146	7	214
16 × 13	Standard ceph	QuickScan+	11.4	12	48	6	8	43	252	44	36	10	186	9	261
8 × 8	Dentition	QuickScan	23.0	19	112	10	8	42	596	28	76	20	384	20	561
16 × 6	Maxilla	QuickScan	19.7	19	68	8	5	46	463	65	72	18	356	16	542
16 × 6	Mandible	QuickScan	34.5	39	164	19	17	81	808	30	109	31	528	30	824
16 × 8	Both arches	QuickScan	39.2	44	177	22	19	92	917	57	125	34	621	34	942
16 × 11	Arches + TMJ	QuickScan	43.4	50	193	24	26	107	972	123	137	37	701	36	1004
16 × 13	Standard ceph	QuickScan	54.5	56	257	30	39	123	1194	216	171	47	907	46	1220
8 × 8	Dentition	Standard	44.5	31	222	22	12	71	1172	58	149	40	780	38	1079
16 × 6	Maxilla	Standard	31.6	29	101	12	11	73	719	131	119	29	629	25	867
16 × 6	Mandible	Standard	61.3	59	290	33	18	124	1567	51	198	54	944	53	1519
16 × 8	Both arches	Standard	69.8	70	329	40	23	150	1693	95	225	61	1131	60	1677
16 × 11	Arches + TMJ	Standard	79.4	81	353	43	41	176	1859	238	256	67	1333	65	1861
16 × 13	Standard ceph	Standard	85.3	83	405	48	74	185	1898	380	265	71	1433	69	1875
8 × 8	Dentition	High resolution	85.1	62	434	42	23	139	2237	115	279	75	1470	73	2012
16 × 6	Maxilla	High resolution	65.0	60	204	23	28	152	1488	276	244	59	1258	52	1809
16 × 6	Mandible	High resolution	126.5	126	620	72	40	263	3131	101	403	114	1972	113	3043
16 × 8	Both arches	High resolution	148.1	148	735	81	50	315	3527	199	473	131	2375	128	3518
16 × 11	Arches + TMJ	High resolution	158.8	161	747	86	71	350	3641	452	508	136	2677	131	3667
16 × 13	Standard ceph	High resolution	171.1	163	821	96	145	365	3809	728	537	144	2899	140	3794
23 × 17	Extended FOV	Standard	69.2	84	301	39	50	202	1293	668	195	53	1038	49	1391
23 × 17	Extended FOV	Enhanced	136.2	170	608	74	97	408	2530	1282	378	103	2027	97	2690

TMJ, Temporomandibular joint; *ceph*, cephalometric.

phantom.[15] In this study, we used both adult and 10-year-old pediatric ATOM phantoms, allowing us to effectively bracket risk and thereby provide estimates that are applicable to the majority of orthodontic patients.

Another novel component of our study was the type of dosimeters that were used. OSL dosimeters can be read within minutes of exposure, allow for multiple nondestructive reads, and can be erased and reused. This is significant because this study would have required more than 1000 separate dosimeters if TLDs had been used, some of which would most likely have failed during the destructive read process. Hence, testing the many FOVs and exposure combinations in

Table VI. Equivalent dose measurements (μGy) on a 10-year-old child phantom for i-CAT FLX by FOV, region of interest, and scanning protocol

				Weighted components of effective dose calculation group components								*Remainder group components*			
FOV (cm)	*Region of interest*	*Protocol*	*Effective dose (μSv)*	*Bone marrow*	*Thyroid*	*Esophagus*	*Skin*	*Bone surface*	*Salivary glands*	*Brain*	*Remainder average*	*Lymphatic nodes*	*Extrathoracic airway*	*Muscle*	*Oral mucosa*
16 × 6	Maxilla	QuickScan+	4.7	2	20	1	7	7	115	25	18	4	93	4	128
8 × 8	Dental	QuickScan+	6.8	3	45	2	3	13	163	12	22	5	116	5	163
16 × 6	Mandible	QuickScan+	9.4	5	78	4	5	21	189	9	27	7	137	7	197
16 × 8	Both arches	QuickScan+	12.3	8	117	5	5	32	212	15	31	8	167	8	222
16 × 11	Arches + TMJ	QuickScan+	13.3	9	121	5	9	34	221	52	34	9	186	9	233
16 × 13	Standard ceph	QuickScan+	17.5	12	160	8	11	46	277	98	42	11	235	11	292
16 × 6	Maxilla	QuickScan	22.8	11	102	7	31	24	541	130	82	19	440	19	592
8 × 8	Dental	QuickScan	33.9	18	242	12	13	42	762	69	106	26	557	26	769
16 × 6	Mandible	QuickScan	42.6	26	355	18	23	64	856	50	122	32	625	32	895
16 × 8	Both arches	QuickScan	50.3	31	412	20	26	74	973	142	143	36	758	36	1023
16 × 11	Arches + TMJ	QuickScan	55.6	36	417	22	42	84	1045	330	156	39	845	39	1103
16 × 13	Standard ceph	QuickScan	69.6	51	637	30	43	120	1085	429	166	44	935	44	1138
16 × 6	Maxilla	Standard	38.7	19	158	11	69	43	889	252	142	30	820	30	969
8 × 8	Dental	Standard	60.1	33	403	20	20	77	1401	134	191	45	1059	45	1331
16 × 6	Mandible	Standard	73.2	41	530	30	34	98	1654	106	224	57	1133	57	1670
16 × 8	Both arches	Standard	85.1	53	659	35	39	126	1754	192	248	62	1343	62	1763
16 × 11	Arches + TMJ	Standard	115.1	80	1001	53	81	190	2045	391	302	77	1713	77	2060
16 × 13	Standard ceph	Standard	120.1	91	1003	53	82	211	2038	731	303	77	1729	77	2054

TMJ, Temporomandibular joint; *ceph*, cephalometric.

the i-CAT FLX would have been less feasible without the OSL dosimeters.

It was important to validate the results obtained with the ATOM phantoms and the OSL dosimeters by comparing them with the more common RANDO phantom and thermoluminescent dosimetry data. The comparisons of TLDs and OSL dosimeters yielded differences of less than 2% in the calculation of effective doses. Likewise, the comparison of the analog vs ATOM phantoms also demonstrated less than a 2% difference in calculated effective dose. These results suggest that our current OSL ATOM adult phantom data can be reasonably compared with data obtained from radiation analog dosimetry phantoms and TLDs.

There is no shortage of controversy surrounding CBCT in orthodontics. Some authors have expressed concern over the trend to use high-dose, high-resolution CBCT scans on young orthodontic patients as a substitute for stone study models or for the automated manufacturing of custom appliances.[16] Relevant to this issue, the results of our study demonstrate that effective doses were an average of 36% greater in the child phantom than in the adult phantom. Not only is the effective dose one third higher, but also, due to the increased radiosensitivity of tissues, the risk is an additional 2 to 5 times higher to a pediatric patient.[5] This is important information to consider when determining what type of diagnostic imaging might be best for a patient. It is also important to consider the cause of differences in the effective dose between the adult and child phantoms. An examination of the equivalent doses to each organ showed that the increase in effective dose in the child was mostly due to the simulated anatomic position of the thyroid (Fig 9). The values calculated for thyroid dose are based on readings from 2 dosimeters positioned at level 10 of the adult ATOM phantom. This is where the bulk of the lobes and the isthmus of the thyroid gland are located. This position is also analogous to the position of dosimeters used in the RANDO phantom, with the exception that both dosimeters are deep in the ATOM phantom, whereas 1 dosimeter was superficial in the RANDO phantom. In contrast, thyroid dose calculation in the child phantom was based on 2 dosimeters in level 9 averaged with 1 dosimeter in level 8. The rationale for this difference in dose measurement was based on the proximity of the thyroid gland to the lower border of the mandible, which is closer in children than in adults (Fig 9). This proximity

Table VII. QUART phantom image measurements

	QuickScan+	*QuickScan*	*Standard*	*High resolution*	*High resolution*	*High resolution*	*QuickScan+*
FOV (mm)	8 × 8	8 × 8	8 × 8	8 × 8	8 × 8	8 × 8	16 × 8
Scan angle (°)	180	180	360	360	360	360	180
Voxel size (mm)	0.3	0.3	0.3	0.125	0.2	0.25	0.3
Averages of 3 measurements							
PMMA voxel	709.4	742.1	733.0	734.5	741.7	740.4	864.7
PMMA noise	105.1	52.5	38.2	88.7	90.7	88.5	96.6
Homogeneity	17.0	18.0	49.0	52.0	63.0	60.0	15.7
Contrast	722.7	724.2	690.4	632.1	644.6	714.6	629.0
CNR	7.7	16.3	22.3	7.0	7.6	9.0	5.8
MTF 10%	1.0	1.1	1.1	1.6	1.3	1.3	0.9
MTF 50%	0.6	0.6	0.6	0.9	0.8	0.7	0.5
Nyquist frequency	1.7	1.7	1.7	4.0	2.5	2.0	1.6
Standard deviations of measurements							
PMMA voxel	1.8	4.8	2.9	1.0	5.1	0.2	2.5
PMMA noise	0.7	0.6	0.3	0.8	1.4	1.0	2.2
Homogeneity	1.0	1.0	4.4	6.1	16.1	2.6	1.2
Contrast	28.9	62.5	6.5	16.9	32.7	56.4	43.8
CNR	1.1	3.1	2.2	0.8	0.5	1.4	0.3
MTF 10%	0.0	0.2	0.1	0.1	0.2	0.4	0.0
MTF 50%	0.0	0.0	0.0	0.1	0.1	0.2	0.0
Nyquist frequency	0.0	0.0	0.0	0.0	0.0	0.0	0.0

PMMA, Polymethylmethacrylate; *CNR*, contrast-to-noise ratio; *MTF*, modulation transfer function.

means that direct exposure of the thyroid is more likely in children than in adults when the base of the FOV is situated just below the chin. Intensity of scatter radiation from jaw structures to the thyroid will also increase with the reduced distance of these structures in a child. Because the thyroid has a tissue weight of 0.04, this organ provides a significant contribution to the calculation of the effective dose for head and neck exposures. With patients, direct thyroid exposure can be reduced by rotating the chin upward and positioning the lower border of the mandible parallel to the rotational plane of the beam (parallel to the floor); however, this strategy was not possible with the ridged phantoms used in this study. It is also important to consider that this strategy, which utilizes the chincup, may cause difficulties for those wishing to do cephalometric analysis of the soft-tissue profile, especially analysis of chin, neck, and throat forms.

After the consideration of patient positioning and proper FOV selection, our data demonstrate that optimization of exposure parameters and filtration can greatly reduce patient dose. We have shown that the QuickScan+ protocol provided a substantial 87% reduction in dose compared with the standard exposure protocols in both child and adult phantoms. Thus, when QuickScan+ protocols can be used, they will provide a clinically meaningful reduction in dose. The largest Quick Scan+ dose recorded in this study (18 μSv) was for the 13 × 16-cm child cephalometric scan. This dose is little more than 2 days of per capita background radiation in the United States. It is also 2 orders of magnitude less than a typical medical computed tomography head scan. The full FOV QuickScan+ protocols are also less than the combined doses of representative modern digital 2-dimensional panoramic and cephalometric radiographs (14-24 and 4 μSv, respectively).[13,17] As a side note, our testing of the i-CAT's 2-dimensional panoramic capabilities known as the iPAN demonstrated a dose of 24 μSv for both the adult and the child phantoms (i-Cat Next Generation, unpublished).

The i-CAT FLX retains its SureSmile (OraMetrix, Richardson, Tex) certification. In 2012, Grunheid et al[17] conducted dosimetry of the SureSmile scan protocol using an i-CAT Next Generation unit. The SureSmile scan protocol requires a high-resolution, 0.2-mm voxel scan. Similar to the results of Grunheid et al, we found that a SureSmile scan of both arches (16 × 8-cm FOV) in an adult imparts an effective dose of 148 μSv. We did not conduct high-resolution imaging of the pediatric phantom; however, we found that pediatric phantom doses were on average 36% greater than adult phantom doses. Hence, the estimated high-resolution SureSmile dose for the average orthodontic patient most likely is between 148 and 198 μSv. In May 2012, OraMetrix announced that they will now accept a "14.7"-second scan instead of the high-resolution "26.9"-second scan, dropping the estimated dose for a 16 × 8-cm SureSmile scan to between 97 μSv and 132 μSv for the average patient.[18]

Table VII. Continued

QuickScan	*Standard*	*QuickScan+*	*QuickScan*	*Standard*	*High-resolution half scan*	*High-resolution half scan*
16 × 8	16 × 8	16 × 8	16 × 8	16 × 8	8 × 8	8 × 8
180	360	180	180	360	180	180
0.3	0.3	0.4	0.4	0.4	0.2	0.25
889.6	890.4	861.1	890.5	886.9	743.7	725.4
50.8	37.7	95.6	50.4	37.1	122.8	122.4
16.0	16.0	17.7	17.0	15.7	15.3	17.0
649.0	627.3	715.5	673.7	635.5	637.0	723.6
11.4	20.6	8.2	16.7	18.2	4.8	6.4
0.9	0.9	0.9	0.9	0.9	1.7	1.6
0.5	0.5	0.5	0.5	0.5	1.0	0.9
1.6	1.7	1.3	1.3	1.2	2.5	2.0
0.9	0.6	1.2	0.3	0.5	33.5	0.6
0.1	2.1	0.9	0.7	1.3	0.5	1.0
1.0	1.0	1.2	1.0	0.6	0.6	1.0
35.8	40.8	43.9	50.9	35.2	4.5	37.4
0.6	1.3	0.5	4.1	0.1	0.4	0.8
0.0	0.0	0.1	0.0	0.0	0.0	0.0
0.0	0.0	0.1	0.0	0.0	0.0	0.0
0.0	0.0	0.0	0.0	0.0	0.0	0.0

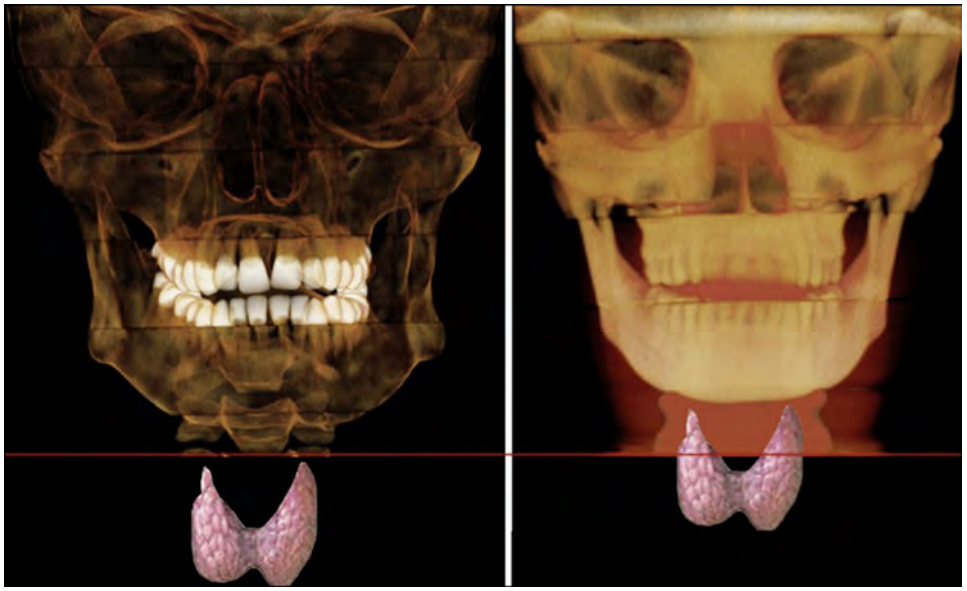

Fig 9. Comparison of thyroid level in child and adult. The *red line* denotes the lower edge of the volume.

In the quest to lower the dose of ionizing radiation administered to patients, dramatic reductions are meaningless if image quality degrades to the point of being nondiagnostic. As optimization and dose reduction become more of a focus for CBCT manufacturers, the effects on image quality will need close attention. Published evidence establishing the usability of low-dose and low-quality scans for diagnostic purposes in dentistry or in orthodontics is limited. However, a potential application specific to orthodontics would be a mid-treatment scan to evaluate root angulations. Additional studies are needed to confirm that other important information in 2-dimensional imaging or higher-dose scans such as gross advances in periodontal conditions,

changes in root length, and changes in morphology that indicate patterns of resorption are not lost in these low-dose scans.

Germany is the first country to develop national standards for image quality testing of dental CBCT devices. The QUART DVT phantom is the first commercially available phantom that complies with those standards. We evaluated the effect of the new Quickscan+ protocols on the objective components of image quality contrast-to-noise ratio and modulation transfer function using the QUART DVT phantom. Our data demonstrated that when voxel size and FOV are held constant, an increase in contrast-to-noise ratio is seen with increasing energy and milliamperes (QuickScan+ <QuickScan <standard). Changes in contrast-to-noise ratio have been shown to generally correlate with observer impressions of an image.[19] As the contrast-to-noise ratio increases, the general impression of how an image appears improves. Changes in voxel size and FOV also influence the contrast-to-noise ratio. As expected, our data demonstrated that increasing the diameter of the FOV resulted in a modest reduction in the contrast-to-noise ratio, whereas increasing the size of the voxel from .3 to .4 mm resulted in an increased contrast-to-noise ratio. Interestingly, with high-resolution scans, increasing voxel size from .125 to .25 mm showed a slight trend of increased contrast-to-noise ratio. This is not dramatic and might not be clinically significant. The reduction of energy and milliamperes from the QuickScan to the QuickScan+ protocols reduced the effective dose to patients by a factor of 4, but only reduced the contrast-to-noise ratio by a factor of 2. Hence, the reduction of energy and milliamperes in the i-CAT FLX was an effective way to reduce patient dose in exchange for a modest reduction in the image quality as measured by the contrast-to-noise ratio. In comparison, the objective measure of resolution, the modulation transfer function, was not as sensitive to the effects of milliamperes but was more sensitive to increases in FOV diameter and voxel size. Although contrast-to-noise ratio and modulation transfer function can be correlated to subjective image quality, additional research to evaluate their influences on diagnostic efficacy is needed.[6]

CONCLUSIONS

The results of this study reflect a large range of imaging options that can be tailored to specific regions of interest. Various exposure options are also available to adjust exposure levels to accommodate a range of diagnostic tasks. Use of QuickScan and QuickScan+ imaging protocols and smaller FOVs result in significant patient dose reductions over alternative larger fields or standard or high-resolution protocols. Practitioners can be guided by selection criteria in deciding which orthodontic patients are most likely to benefit from a radiographic examination and which examination is most likely to provide the needed information. Such guidelines consider the balance of benefit and potential harm from diagnostic imaging. A working group of orthodontists and oral and maxillofacial radiologists has developed initial guidelines that have been adopted in a position paper by the American Academy of Oral and Maxillofacial Radiology.[20] Determination of which exposure protocol is appropriate for a specific diagnostic task awaits further research. Contrast-to-noise ratio data in conjunction with modulation transfer function indications of resolution limits might be helpful guides in indicating the usefulness of different scanning parameters for specific diagnostic tasks.

REFERENCES

1. Kapila S, Conley RS, Harrell WE Jr. The current status of cone beam computed tomography in orthodontics. Dentomaxillofac Radiol 2011;40:24-34.
2. Smith-Bindman R, Lipson J, Marcus R, Kim KP, Mahesh M, Gould R, et al. Radiation dose associated with common computed tomography examinations and the associated lifetime attributable risk of cancer. Arch Intern Med 2009;169:2078-86.
3. Ludlow JB, Ivanovic M. Comparative dosimetry of dental CBCT devices and 64-slice CT for oral and maxillofacial radiology. Oral Surg Oral Med Oral Pathol Oral Radiol Endod 2008;106:106-14.
4. Brenner DJ, Hall EJ. Computed tomography—an increasing source of radiation exposure. N Engl J Med 2007;357:2277-84.
5. Brenner D, Elliston C, Hall E, Berdon W. Estimated risks of radiation-induced fatal cancer from pediatric CT. AJR Am J Roentgenol 2001;176:289-96.
6. Watanabe H, Honda E, Tetsumura A, Kurabayashi T. A comparative study for spatial resolution and subjective image characteristics of a multi-slice CT and a cone-beam CT for dental use. Eur J Radiol 2011;77:397-402.
7. Valentin J. The 2007 recommendations of the International Commission on Radiological Protection. Publication 93. Ann ICRP 2007;37:1-332.
8. Underhill TE, Chilvarquer I, Kimura K, Langlais RP, McDavid WD, Preece JW, et al. Radiobiologic risk estimation from dental radiology. Part I. Absorbed doses to critical organs. Oral Surg Oral Med Oral Pathol 1988;66:111-20.
9. Cristy M. Active bone marrow distribution as a function of age in humans. Phys Med Biol 1981;26:389-400.
10. Physical aspects of irradiation. NBS handbook 85. Washington, DC: US Government Printing Office; 1963.
11. Ludlow JB, Davies-Ludlow LE, Brooks SL. Dosimetry of two extraoral direct digital imaging devices: NewTom cone beam CT and Orthophos Plus DS panoramic unit. Dentomaxillofac Radiol 2003;32:229-34.
12. Ludlow JB, Davies-Ludlow LE, Brooks SL, Howerton WB. Dosimetry of 3 CBCT devices for oral and maxillofacial radiology: CB Mercuray, NewTom 3G and i-CAT. Dentomaxillofac Radiol 2006;35:219-26.

13. Ludlow JB, Davies-Ludlow LE, White SC. Patient risk related to common dental radiographic examinations: the impact of 2007 International Commission on Radiological Protection recommendations regarding dose calculation. J Am Dent Assoc 2008; 139:1237-43.
14. Pauwels R, Beinsberger J, Stamatakis H, Tsiklakis K, Walker A, Bosmans H, et al. Comparison of spatial and contrast resolution for cone-beam computed tomography scanners. Oral Surg Oral Med Oral Pathol Oral Radiol 2012;114:127-35.
15. Cassola VF, Milian FM, Kramer R, de Oliveira Lira CA, Khoury HJ. Standing adult human phantoms based on 10th, 50th and 90th mass and height percentiles of male and female Caucasian populations. Phys Med Biol 2011;56:3749-72.
16. Bogdanich W, Craven McGinty J. Radiation worries for children in dentists' chairs. The New York Times (NY ed) 2010 Nov 23;Sect. A:1.
17. Grunheid T, Kolbeck Schieck JR, Pliska BT, Ahmad M, Larson BE. Dosimetry of a cone-beam computed tomography machine compared with a digital x-ray machine in orthodontic imaging. Am J Orthod Dentofacial Orthop 2012;141:436-43.
18. OraMetrix & Imaging Sciences Announce Lower Dose, Faster i-CAT® Scan for SureSmile Orthodontic Treatment Planning. Available at http://www.suresmile.com/About-SureSmile/SureSmile-In-The-News/Press-Releases/OraMetrix–Imaging-Sciences-Announce-Lower-Dose–. Accessed October 18, 2013.
19. Lin Y, Wang X, Sehnert WJ, Foos DH, Barski L, Samei E. Quantification of radiographic image quality based on patient anatomical contrast-to-noise ratio: a preliminary study with chest images. Proc. SPIE 7627, Medical Imaging 2010: Image Perception, Observer Performance, and Technology Assessment, 76271F (March 3, 2010).
20. American Academy of Oral and Maxillofacial Radiology. Clinical recommendations regarding use of cone beam computed tomography (CBCT) in orthodontics. Position statement by the American Academy of Oral and Maxillofacial Radiology. Oral Surg Oral Med Oral Pathol Oral Radio 2013;116:238-57.